JACS
JOURNAL OF THE AMERICAN CHEMICAL SOCIETY

ARTICLE

pubs.acs.org/JACS

Probing the Photoinduced Metal−Nitrosyl Linkage Isomerism of Sodium Nitroprusside in Solution Using Transient Infrared Spectroscopy

Michael S. Lynch, Mark Cheng, Benjamin E. Van Kuiken, and Munira Khalil*

Department of Chemistry, University of Washington, Seattle, Washington 98195, United States

Supporting Information

ABSTRACT: We study photoinduced metal−nitrosyl linkage isomerism in sodium nitroprusside ($Na_2[Fe^{II}(CN)_5NO]\cdot 2H_2O$, SNP) dissolved in methanol using picosecond transient infrared (IR) spectroscopy. The high sensitivity of this technique allows the simultaneous observation of two known metastable (MS) iron−nitrosyl linkage isomers of SNP, $[Fe^{II}(CN)_5(\eta^1\text{-ON})]^{2-}$ (MS1) and $[Fe^{II}(CN)_5(\eta^2\text{-NO})]^{2-}$ (MS2), at room temperature. The transient population of free nitrosyl radicals (NO·) is also measured in the sample solution. These three transient species are detected using their distinct nitrosyl stretching frequencies at 1794 cm^{-1} (MS1), 1652 cm^{-1} (MS2), and 1851 cm^{-1} (NO·). The metastable isomers and NO· are formed on a subpicosecond time scale and have lifetimes greater than 100 ns. A UV (400 nm)−pump power dependence study reveals that MS1 can be formed with one photon, while MS2 requires two photons to be populated at room temperature in solution. Other photodissociation products including cyanide ion, Prussian blue, and $[Fe^{III}(CN)_5(CH_3OH)]^{2-}$ are observed. We develop a photochemical kinetic scheme to model our data, and the analysis reveals that photoisomerization and photodissociation of the metal−NO moiety are competing photochemical pathways in SNP dissolved in methanol at room temperature. Based on the analysis, the solvent-associated Fe(III) species and Prussian blue form on a 130 and 320 ps time scale, respectively. The simultaneous detection and characterization of photoinduced linkage isomerism (MS1 and MS2) and photodissociation of the metal−NO bond in SNP highlights the importance of understanding the role played by metastable metal−nitrosyl linkage isomers in the photochemistry of metal−nitrosyl compounds in chemistry and biology.

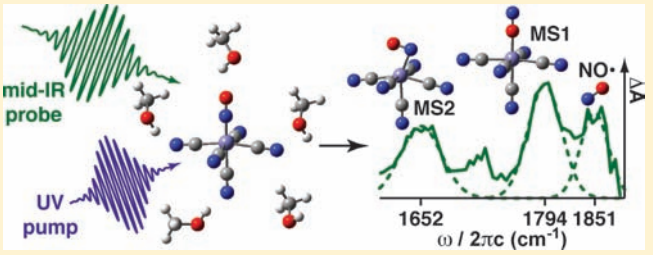

INTRODUCTION

Photoinduced linkage isomerism in metal−nitrosyl compounds is a rich field of study in which irradiation of the sample by light causes the nitrosyl ligand to bond to the metal center in multiple ways.[1−5] There are three limiting binding forms of the metal−nitrosyl moiety. The metal−NO species with the nitrogen atom bound to the metal is observed in the electronic ground state (GS). Upon photoexcitation, the nitrosyl ligand can rotate by 180° to form the metal−ON (isonitrosyl) species or by 90° to form the η^2-NO ligand bound to the metal in a side-on geometry as illustrated in Figure 1. To date, photoinduced linkage isomerism has been documented in several transition metal−nitrosyl species, and there is great interest in understanding how the metal−NO coordination of these species relates to the overall photochemistry of the compound including NO release pathways.[6−9] Studies on nitrosyl porphyrins and nitrosyl heme proteins have also discovered metastable linkage isomers, underlining the importance of understanding the role played by metal−nitrosyl isomers in nitric oxide signaling pathways in biological systems.[10−15]

Sodium nitroprusside ($Na_2[Fe^{II}(CN)_5NO]\cdot 2H_2O$, SNP) is a prototypical system for studying photoinduced metal−nitrosyl linkage isomerism. Approximately 30 years ago, SNP was found to exhibit at least two long-lived electronic excited states following photoexcitation with 350−580 nm radiation.[16,17] The exact nature of these photoinduced metastable states (MS) remained unknown until Coppens and co-workers identified and characterized two unique MS linkage isomers formed upon photoexcitation of a single crystal of SNP using low-temperature X-ray crystallography.[18−20] One of the linkage isomers contained an isonitrosyl group (MS1), while the other involved an η^2-NO ligand (MS2) bound to the iron core (Figure 1). The discovery of photoinduced linkage isomerism occurring in crystalline SNP generated significant interest for its use in high capacity optical storage devices due to the large change of refractive index upon irradiation with light.[5,21−27] Along with creating metastable linkage isomers, the photoexcitation of SNP can result in the dissociation of the nitrosyl ligand. This property is utilized in the medical community where aqueous SNP is used as an NO delivery agent in extreme hypertensive emergencies.[28−31]

Given its possible uses, photoinduced linkage isomerism in SNP has garnered intense experimental and theoretical attention over the past decades as summarized in several recent

Received: April 29, 2010
Published: March 18, 2011

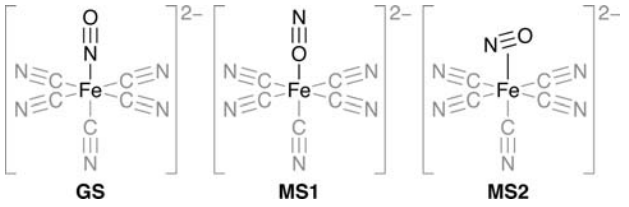

Figure 1. Structure of the GS, MS1, and MS2 of the nitroprusside ion highlighting Fe−NO linkage isomerism.

reviews.[1,5,32] The experimental study of photoinduced linkage isomerism has mainly focused on the solid state where the metastable species can be trapped at low temperatures and subsequently characterized with steady-state spectroscopic and structural probes.[20,33−43] An exception to this is work by Schaniel et al. where nanosecond transient absorption experiments on SNP in aqueous solutions detected the formation of MS2 with a lifetime of ∼110 ns.[44] Experiments photoexciting aqueous solutions of SNP with continuous wave radiation have shown the formation of several dissociation products including the nitrosyl radical (NO·), cyanide ion (CN^-), $[Fe^{III}(CN)_5(H_2O)]^{2-}$, and Prussian blue (PB).[45−48] Theoretical works have calculated the electronic absorption spectra of the GS, MS1, and MS2 species and have considered the energetics of photoinduced linkage isomerism occurring on a multidimensional potential energy surface.[43,49−55] The theoretical studies along with the trapping of the linkage isomers using light of different wavelengths have suggested that the formation of MS1 and MS2 requires more than one photon depending on the experimental temperature.[20,54]

Despite the rich history of studying SNP, important questions remain unanswered regarding the formation of photoinduced metastable states in solution. Can both MS1 and MS2 be populated at room temperature in solution? What are their lifetimes? What role do the linkage isomers play in the photogeneration of NO radical and other photodissociation products? The goal of this study is to answer the questions listed above and provide a detailed understanding of the photochemistry of SNP in solution at room temperature, which is currently lacking.

In this Article, we use picosecond transient infrared (IR) spectroscopy to probe the photoinduced linkage isomers and related photoproducts of SNP generated at room temperature with a 400 nm pump pulse. The photoinduced MS1 and MS2 species have nitrosyl stretching frequencies distinct from the ground state of SNP, allowing us to probe their structural dynamics on a picosecond time scale. We directly observe the formation of both MS1 and MS2 linkage isomers of SNP at room temperature in a methanol solution and find that their lifetimes are greater than 100 ns. The 400 nm pump power dependence reveals that MS1 is formed via a one-photon process while the formation of MS2 requires two photons. In addition to Fe−NO linkage isomers, photodissociation products including NO·, CN^-, Prussian blue, and $[Fe^{III}(CN)_5(CH_3OH)]^{2-}$ are observed, and their picosecond dynamics are measured. We construct a photochemical model based on our data, which reveals that photoinduced linkage isomerism and photodissociation of the nitrosyl ligand are competing photochemical pathways when SNP is dissolved in methanol at room temperature.

MATERIALS AND METHODS

Materials. All chemical samples were purchased from Sigma-Aldrich Co. and were used without further purification. Solutions of SNP dissolved in methanol were prepared under ambient conditions (295 K) to concentrations of 120 or 60 mM for experiments in the NO (1600−2000 cm^{-1}) or CN (2000−2200 cm^{-1}) stretching regions, respectively. Figure 2 shows the UV/vis and FTIR spectra of SNP in methanol. The optical absorption spectrum of SNP displays two resonances at 393 and 520 nm assigned as the 7e ← 6e [π^*(NO) ← $3d_{xz,yz}$] and 7e ← $2b_2$ [π^*(NO) ← $3d_{xy}$] transitions, respectively.[43,49] The UV/vis spectrum was obtained using a JASCO V-630 spectrometer with 1 nm resolution. The solvent-subtracted FTIR spectrum of SNP in methanol shows peaks corresponding to the nitrosyl stretch (ν_{NO}) and the cyanide stretches (ν_{CN}) centered at 1909 cm^{-1} ($\varepsilon = \int \varepsilon_\nu d\nu = 3.3 \times 10^4$ M^{-1} cm^{-2}) and 2145 cm^{-1}. The asymmetric ν_{CN} band contains contributions from multiple IR active modes corresponding to the C_{4v} symmetry of the molecule,[56] with an E mode centered at 2144 cm^{-1} ($\varepsilon = 4.8 \times 10^3$ M^{-1} cm^{-2}) and A_1 modes centered at 2155 cm^{-1} ($\varepsilon = 3.7 \times 10^3$ M^{-1} cm^{-2}). The IR spectrum was obtained using a JASCO FT/IR-4100 spectrometer with 2 cm^{-1} resolution.

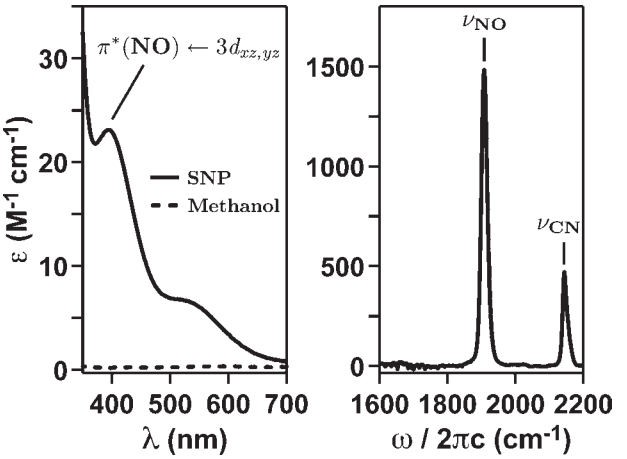

Figure 2. (Left) UV/vis spectra of SNP in methanol (−) and neat methanol (− − −) at T = 295 K. (Right) Solvent-subtracted FTIR spectrum of SNP dissolved in methanol. The center frequencies for ν_{NO} and ν_{CN} are 1909 and 2145 cm^{-1}, respectively.

Transient Infrared Spectroscopy. The experiment is performed in a pump−probe geometry. The optical pump and the IR probe pulses are derived from the output of a commercial Spectra Physics regenerative amplifier (800 nm, 35 fs, 3 W).

The 400 nm pump pulse is generated by frequency doubling ∼1 W of the 800 nm pulse in a 0.5 mm BBO crystal. To minimize multiphoton effects in the solvent and nonlinear processes on the sample windows, the pulse is stretched to ∼850 fs by passage through 5.5 cm of fused silica. The pump pulse energy at the sample is ∼40 μJ (80 μJ) over a focal spot-size of ∼430 μm (500 μm) resulting in a pump fluence of ∼28 mJ/cm^2 (∼41 mJ/cm^2) for experiments probing the NO (CN) regions. The polarization and input energy of the pump pulse is controlled using a half-waveplate and a calcite polarizer. The mid-IR probe pulse is obtained by sending ∼1 W of the 800 nm light to pump a two-pass optical parametric amplifier. The signal and idler fields are then difference-frequency mixed in a 0.5 mm $AgGaS_2$ crystal to produce ∼60 fs mid-IR pulses with spectral bandwidths greater than 250 cm^{-1} at center wavelengths of 4.6 and 5.6 μm. The IR probe is focused to a spot size of 190 μm at the sample with an energy of ∼0.5 μJ per pulse.

The pump and probe pulses spatially and temporally overlap at the sample that is held between two 1 mm thick CaF_2 windows with a 50 μm Teflon spacer in a home-built flow cell. A sample volume of 60 mL is mechanically pumped through the cell at rate of ∼1 m/s, and the sample cell is translated in the sample plane at 0.125 mm/s. A computer-controlled translation stage in the pump arm controls the relative time delay between the UV-pump and IR-probe with a maximum time delay

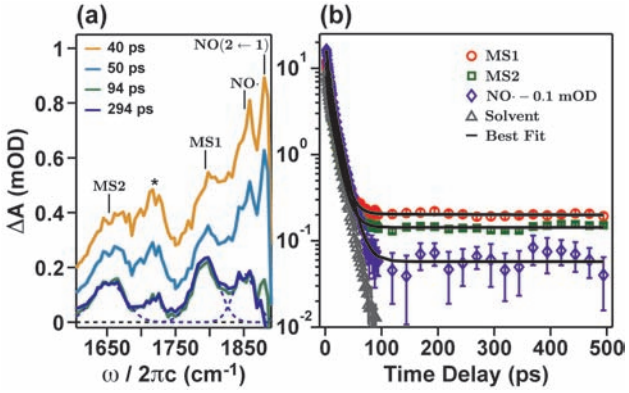

Figure 3. (a) Picosecond transient IR spectra of SNP in methanol in the NO stretching region at four pump−probe time delays. The peak labeled NO(2 ← 1) refers to the transient absorption of the NO overtone in the GS. Dotted lines are Gaussian fits of MS1 (ω_c = 1794 cm^{-1}), MS2 (ω_c = 1652 cm^{-1}), and NO· (ω_c = 1851 cm^{-1}) IR lineshapes at a time delay of 294 ps. Here, ω_c refers to the central frequency of the Gaussian lineshapes. The feature marked with an asterisk is due to solvent background. (b) Kinetics in the NO stretching region with best fit. The NO radical has been shifted by −0.1 mOD for clarity.

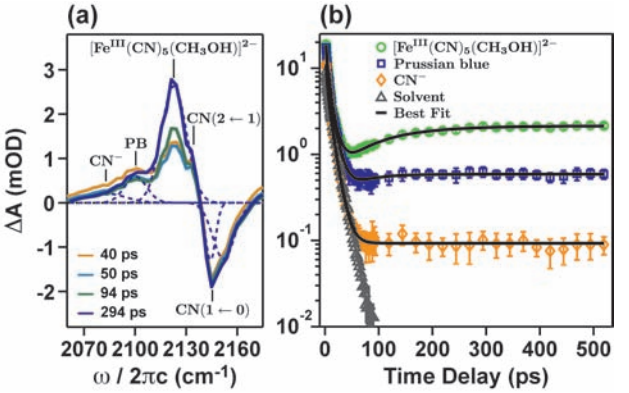

Figure 4. (a) Time-resolved IR absorption spectra of SNP in methanol in the CN stretching region at four time delays. Dotted lines are Gaussian fits of CN$^-$ (ω_c = 2083 cm^{-1}), PB (ω_c = 2100 cm^{-1}), and [Fe^{III}(CN)$_5$(CH$_3$OH)]$^{2-}$ (ω_c = 2123 cm^{-1}) at a time delay of 294 ps. The CN bleach [CN(1← 0)] has been fit using the FTIR spectrum of SNP in methanol (Figure 1). The peak labeled CN(2 ← 1) refers to the transient absorption of the CN overtone of the GS. (b) Kinetics in the CN stretching region with best fit.

of 500 ps. The polarization of the pump pulse is set to magic angle (54.7°) with respect to the probe pulse to selectively sample the isotropic vibrational dynamics. Transient IR difference spectra are collected with a mechanical chopper operating at 500 Hz in the pump arm. A portion of the probe field is split to create a reference field used for performing shot-to-shot normalization of the IR intensity fluctuations. After the sample, the pump is blocked and the vertically displaced probe and reference fields are sent through a 190 mm spectrometer. The signal is detected at the focal plane of a 2 × 64 element HgCdTe array IR detector with a spectral resolution of ∼4 cm^{-1} (3 cm^{-1}) across the NO (CN) spectral regions. Our instrument response time is ∼1 ps. The signals are averaged over 2500 laser shots, and each kinetic trace is averaged 7−30 times depending on the signal level. This apparatus detects differences in optical density as low as 40 μOD. Error in the data is shown at the 95% confidence level unless otherwise stated. The kinetic traces shown in Figures 3b and 4b are obtained by summing over the full-width at half-maximum (fwhm) of the transient spectral lineshapes.

RESULTS

NO Stretching Region (1600−2000 cm^{-1}). Figure 3a shows time-resolved difference spectra of 120 mM SNP in methanol on a picosecond time scale in the NO stretching region at various pump−probe time delays. The spectra consist of several positive spectral features corresponding to transient photoproducts formed upon photoexcitation at 400 nm. We observe the transient infrared absorbance of the nitrosyl stretch (ν_{NO}) for the MS1 and MS2 photoinduced linkage isomers at 1794 and 1652 cm^{-1}, respectively. The assignments are based on previously reported ν_{NO} downshifts of approximately 100 and 250 cm^{-1} with respect to the GS for MS1 and MS2, respectively, in SNP and other metal−nitrosyl species at low temperatures.[4,40,41]

Along with the metastable linkage isomers, we observe nitrosyl radical (NO·) generation with the presence of a transient absorption at 1851 cm^{-1}. This frequency corresponds to the stretching frequency of NO· and has a Gaussian line width of 23 cm^{-1}. We assign this frequency on the basis of previous work of NO· in aqueous solutions.[57] The transient absorption from the ν_{NO} overtone (v = 2 ← v = 1) of the GS of SNP peaks at 1881 cm^{-1}, as it is downshifted by the vibrational anharmonicity of 28 cm^{-1} for the NO stretch.[58] A negative spectral feature at 1909 cm^{-1} corresponding to the bleach of the GS species is shown in Figure S1 of the Supporting Information.

Figure 3b displays the measured dynamics of the photochemically generated transient species MS1, MS2, and NO·. The black solid lines are fits to the data with a sum of three exponential functions. The complete results from the fits are tabulated in Table S1 in the Supporting Information. All transient species exhibit an initial biexponential decay with ∼3 and ∼12 ps time constants. We attribute these time scales to the decay of the resonant solvent (see Figure S2) and the nonresonant CaF_2 window response following photoexcitation of the sample at 400 nm. We measure the same time constants (gray triangles in Figure 3b at ω = 1909 cm^{-1}) when we excite a sample containing only methanol with all other experimental conditions remaining the same.

The lifetimes of the photoinduced metastable states and NO· at room temperature in solution are found to be greater than 100 ns as given by the third time constant extracted from the fits.[59] This long time constant is consistent with the work of Schaniel et al., who found that MS2 decays on a 110 ± 10 ns time scale when an aqueous SNP solution is pumped at 532 nm.[44] However, they were not able to detect the presence of MS1 species in their experiment. The ν_{NO} bleach of the GS shows no recovery on the time scale of the experiment, while the ν_{NO} overtone of the GS relaxes back to the vibrational ground state on a 32 ± 7 ps time scale (see Figure S1).

CN Stretching Region (2000−2200 cm^{-1}). Figure 4a displays transient IR spectra following the photoexcitation of 60 mM SNP dissolved in methanol in the CN stretching region at various pump−probe time delays. The transient spectra show four positive features at 2083, 2100, 2123, and 2133 cm^{-1} corresponding to various photoproducts that absorb in the CN region. The largest transient feature in Figure 4a at 2123 cm^{-1} grows as a function of the pump−probe time delay. This is the CN stretch frequency (ν_{CN}) of [Fe^{III}(CN)$_5$(CH$_3$OH)]$^{2-}$, which is generated as a result of NO dissociation and subsequent solvent association at the vacant site.[47] The transient feature at

dx.doi.org/10.1021/ja110881n |J. Am. Chem. Soc. 2011, 133, 5255–5262

2100 cm^{-1} corresponds to the ν_{CN} of the mixed valence compound Prussian blue.[60] The transient spectral feature at 2083 cm^{-1} is the CN stretching frequency of the free cyanide ion (CN^-).[61]

The dynamics of the transient species in the CN stretching region are shown in Figure 4b. The solid lines are fits to a sum of two decaying and one rising exponential function. For the detailed list of kinetic parameters, see Table S3. As in the NO stretching region, there is an initial biexponential decay of ~3 and ~12 ps time scale resulting from resonant solvent and nonresonant CaF_2 window response (gray triangles in Figure 4b at ω = 2145 cm^{-1}). It is clear from Figure 4b that the transient populations of both $[Fe^{III}(CN)_5(CH_3OH)]^{2-}$ and PB are increasing with time. In the case of the cyanide ion, any rise is within the error of the experiment. The data for the solvent-associated species $[Fe^{III}(CN)_5(CH_3OH)]^{2-}$ are fit with a rise time of 95 ± 9 ps, which represents the time scale of a diffusion-limited solvent association process.[62] The transient population of all species remains constant on the time scale of our measurement as seen by the long-time offset.

Note that we do not see signatures of the photoinduced linkage isomers in the CN stretching region. This is because the ν_{CN} in MS1 and MS2 is expected to downshift by only ~10 cm^{-1} with respect to the ground state.[39−41] Given the spectral congestion of other photoproducts in that region and the very small concentration of MS1 and MS2, we do not expect to observe the peaks corresponding to MS1 and MS2 in the CN stretching region.

UV-Pump Power Dependence. To determine whether the formation of the photoinduced linkage isomers is a result of one- or two-photon processes, we perform a UV-pump power dependence in the NO stretching region over a 400 nm pump fluence range of 14−52 mJ/cm^2. The results are shown in Figure 5 where the area of the transient peaks is graphed versus the excitation fluence on a log−log scale plot. Here, the slope (m) of the best-fit line indicates whether the species is formed by a one- (m = 1) or two- (m = 2) photon process. A slope between 1 and 2 represents a combination of both processes.[63] The data reveal that MS1 is formed via a one-photon mechanism (m = 0.9 ± 0.1), whereas MS2 is formed via a two-photon process (m = 1.9 ± 0.2). Free nitrosyl radical is formed from a combination of both one- and two-photon processes (m = 1.4 ± 0.2).

Extracting the Integrated Molar Absorption Coefficient for the Nitrosyl Stretch of MS1, MS2, and NO Radical. Given the low oscillator strength of the 7e ← 6e [π^*(NO) ← $3d_{xz,yz}$] metal-to-ligand charge transfer (MLCT) transition at 400 nm ($\varepsilon_{400\ nm} \approx 23\ M^{-1}\ cm^{-1}$), the total photoexcitation yield of SNP is ~2% even at the relatively high fluence used in this experiment. The population of the metastable states accounts for less than 0.1% of the total quantum yield. The photodissociation of SNP leading to nitrosyl radical generation is the dominant photochemical pathway, which is consistent with previous studies.[45,47,48]

The molar absorption coefficients of the NO stretches for the MS linkage isomers are estimated by taking the ratio of oscillator strengths of GS, MS1, and MS2 calculated using Gaussian 03 and normalizing them with the experimentally obtained value for the GS.[64,65] On the basis of these estimates, we calculate the transient concentrations of MS1, MS2, and NO· at long delay times to be 0.047, 0.040, and 1.2 mM, respectively. The integrated molar absorption coefficients for MS1 and MS2 are found to be ε_{MS1} = 4.4 ± 0.3 × $10^4\ M^{-1}\ cm^{-2}$ and ε_{MS2} = 2.0 ± 0.1 × $10^4\ M^{-1}\ cm^{-2}$, respectively. See the Supporting Information for more computational details.

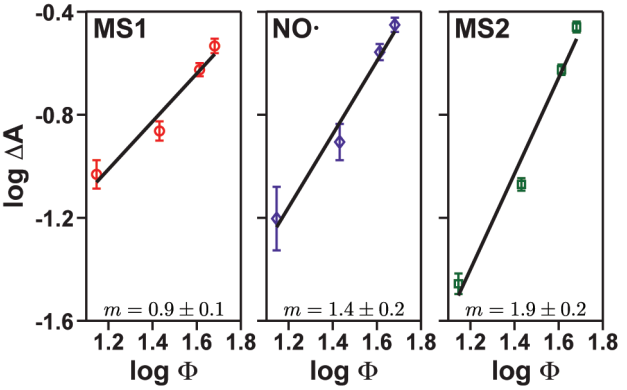

Figure 5. UV-pump power dependence of transients in the NO stretching region (MS1, MS2, NO·) at a time delay of 500 ps presented on a log−log scale plot of transient IR absorption signal (ΔA) versus fluence (Φ, mJ/cm^2). Slope (m) error is shown as the standard error of the linear fit.

The infrared spectrum of the free NO radical is difficult to isolate in solution at room temperature because of its propensity to dimerize at low concentrations.[66] Therefore, the characterization of the vibrational spectrum of NO radical in solution has eluded researchers. A recent study has predicted the integrated absorption coefficient for ν_{NO} of the NO radical to be 200 $M^{-1}\ cm^{-2}$ in solution.[67] The data collected in this experiment allow a direct estimate of the integrated absorption coefficient of ν_{NO} of NO· in methanol to be $\varepsilon_{NO\cdot}$ = 170 ± 20 $M^{-1}\ cm^{-2}$.

DISCUSSION

Most experiments probing metal−nitrosyl linkage isomerism in SNP have been done at very low temperatures to trap the photoinduced metastable states for characterization with X-ray crystallography and various spectroscopies. On the other hand, the generation of NO radical and CN^- following the irradiation of aqueous SNP with continuous-wave light has been studied at room temperature. This work brings these two disparate experimental camps together by performing a detailed time-resolved investigation of the photochemistry of SNP dissolved in methanol at room temperature using picosecond transient infrared spectroscopy.

Transient IR Spectra of the ν_{NO} of MS1, MS2, and NO Radical. For the first time, both metal−nitrosyl linkage isomerism and nitrosyl radical generation has been simultaneously observed at room temperature in solution. Table 1 lists a comparison of the nitrosyl stretching frequencies of the linkage isomers of SNP and the photogenerated NO radical under different experimental conditions.

The significant frequency shift of the ν_{NO} for the two metastable species with respect to the ground state arises from the changes in π backbonding as a result of the rotation of the NO ligand. There are strong π backbonding interactions through the π^* orbital of NO^+ in MS1, although orbital overlap is less efficient than in the GS due to the smaller contribution of the oxygen atom to the π^*(NO) orbital. On the other hand, the symmetry of MS2 (C_s) only allows for π backbonding through one of the Fe 3d orbitals.[54] A reduction in π backbonding results in a lower NO stretching frequency,[68] which is apparent from the trend in the observed stretching frequencies of the GS, MS1, and MS2 listed in all three rows of Table 1.

Table 1. Nitrosyl Stretching Frequencies (cm^{-1}) of SNP under Different Experimental Conditions

T (K)	GS (ε, M^{-1} cm^{-2})	MS1 (ε, M^{-1} cm^{-2})	MS2 (ε, M^{-1} cm^{-2})	NO· (ε, M^{-1} cm^{-2})	reference
295[a]	1909 (3.3×10^4)	1794 (4.4×10^4)	1652 (2.0×10^4)	1851 (1.7×10^2)	this work
77[b]	1960	1835	1664		41
20[c]	1953	1835	1663		39

[a] In methanol solution with λ_{pump} = 400 nm. [b] Suspended solid (Nujol) with λ_{pump} = 488 nm to obtain GS + MS1 and λ_{pump} = 1064 nm to obtain GS + MS2. [c] Single crystal ($E \| c$) with λ_{pump} = 488 nm.

Table 1 shows that the relative downshifts in the ν_{NO} for MS1 and MS2 from the ν_{NO} of the GS measured in this experiment are similar to what has been reported for solid-state samples at low temperatures. The Gaussian line widths of the nitrosyl stretches for MS1, MS2, and the GS in methanol are 40, 45, and 21 cm^{-1}, respectively. The NO stretching frequencies of GS, MS1, and MS2 listed in Table 1 clearly illustrate the influence of the solvent. The primary hydrogen-bonding interactions between the solvent and SNP occur through the more negatively charged cyano ligands, which modulates the NO π backbonding through the metal center.[56,69] It is this shift in electron density resulting in reduced Fe−NO π backbonding that changes the ν_{NO} frequency in the GS, MS1, and MS2 when solvated by methanol molecules. As expected from the coordination geometry of the metal−NO moiety, the solvent-induced frequency shifts are seen most strongly in the GS and MS1 species.

Role of MS1 and MS2 in the Photochemistry of SNP. Using the results from the UV-pump power dependence as described in the previous section, we have built a kinetic model (see Scheme 1) to understand the photochemistry of SNP in methanol at room temperature. The absorption of a 400 nm photon by the GS puts the system in an excited-state manifold labeled GS*. From this state(s), the molecule can undergo an intramolecular rearrangement to form MS1 or dissociate to form $[Fe^{III}(CN)_5]^{2-}$ and NO radical. On absorbing another 400 nm photon from GS*, the molecule can reach a second excited-state manifold labeled X. From this state(s), the molecule can rotate the metal−nitrosyl bond to form MS2 or dissociate into $[Fe^{III}(CN)_5]^{2-}$ and NO radical. The solvent associated species, $[Fe^{III}(CN)_5(CH_3OH)]^{2-}$, Prussian blue, and CN^-, are assumed to form after NO radical photodissociation. The metastable linkage isomers, MS1 and MS2, eventually relax back to the GS. We do not include interconversion between MS1 and MS2 and geminate recombination of NO because we do not observe these processes in our experiment. We view the excited states GS* and X representing multidimensional potential energy surfaces, from which many crossings or seams can be accessed. We note that our experimental time-resolution of ~1 ps does not allow us to uniquely identify GS* and X through their IR signatures. The photochemical scheme described above accounts for the fact that MS1 is formed via a one-photon interaction, MS2 is formed via a two-photon process, and NO radical is formed via a combination of one- and two-photon pathways.

Using Scheme 1 and the aforementioned assumptions, we generate a set of 10 coupled differential equations that are solved numerically. We iteratively fit this model to our solvent-subtracted data set using a nonlinear least-squares algorithm with the assumption that only the GS is populated before the 400 nm pump pulse arrives. A more detailed discussion on the model, the fitting procedure, and the fit results can be found in the Supporting Information.

Scheme 1. Proposed Kinetic Model for the Simultaneous Photochemical Formation of the Observed Linkage Isomerism Products (MS1, MS2) and Dissociation Products (NO·, $[Fe^{III}(CN)_5(CH_3OH)]^{2-}$, CN^-, and Prussian Blue)[a]

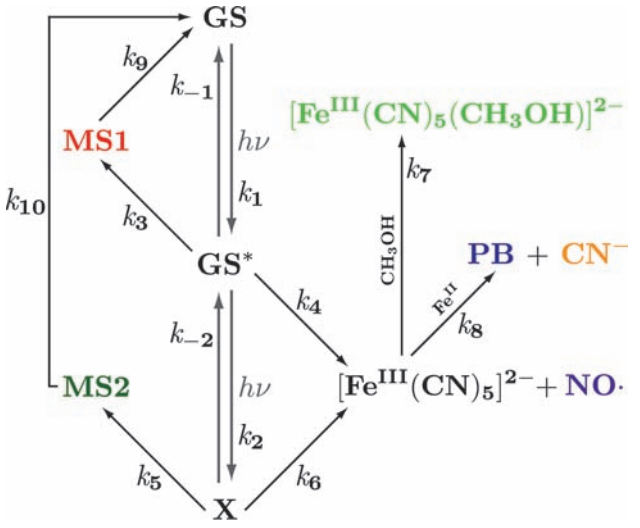

[a] Rates (k_i) are shown beside each corresponding kinetic step, and single photon interactions are written as $h\nu$. The Fe^{II} species needed to generate PB is meant to represent any iron(II) species present in the sample, such as an SNP molecule that has not undergone photoexcitation.

Figure 6 presents the fit results of the model (solid lines) with the solvent-subtracted data (points). Figure 6a displays the concentration of MS1, MS2, and NO radical obtained using the data from the NO stretching region. The inset shows the formation of the three species on a ~300 fs time scale. This is consistent with a recent study, which found that MS2 was formed on a 300 fs time scale in single crystals of SNP at 296 K.[70] We stress that the ultrafast rate constants (k_{1-6}) cannot be assigned uniquely because the solvent background response dominates the early time data. We see that MS1, MS2, and NO· reach their maximum concentration by ~1.5 ps and remain constant over the time scale of the experiment. Figure 6b shows the concentration of the dissociation products $[Fe^{III}(CN)_5(CH_3OH)]^{2-}$, PB, and CN^- increasing as a function of the experimental time delay. From the model, we extract the methanol association rate of $k_7 = (130\ ps)^{-1}$, which is consistent with diffusion-limited association of a methanol molecule into the vacant site of $[Fe^{III}(CN)_5]^{2-}$. The rate of formation of Prussian blue is slower, with $k_8 = (320\ ps)^{-1}$, due to the lower concentration of the iron(II) species in solution. Figure 6c shows model predictions for the early time dynamics of the GS and the three chemical intermediates (GS*, X, and $[Fe^{III}(CN)_5]^{2-}$) not observed in the experiment.

dx.doi.org/10.1021/ja110881n | J. Am. Chem. Soc. 2011, 133, 5255–5262

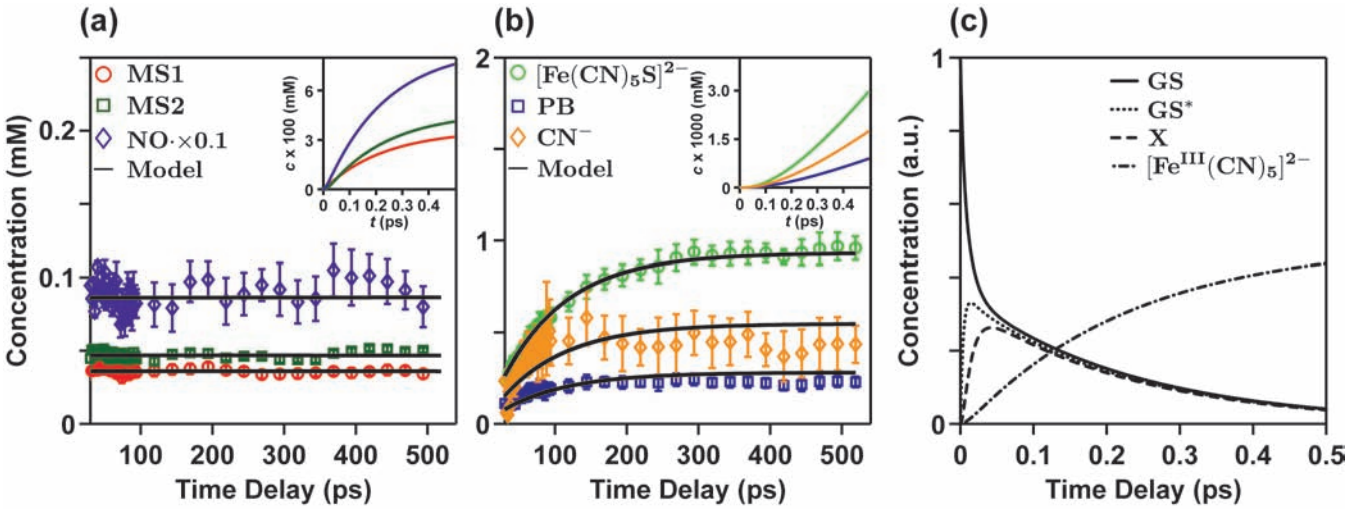

Figure 6. Results of fitting the photochemical kinetic model presented in Scheme 1 to the solvent-subtracted experimental data. (a) Transient concentrations of photochemical species observed in the NO stretching region. Early time dynamics (model only) are shown in the inset. (b) Transient concentrations of the photodissociated products observed in the CN stretching region. Early time dynamics (model only) are shown in the inset. Here, S represents solvent (methanol). (c) Early time dynamics of the intermediate species as predicted by the model in Scheme 1.

The model predicts that the GS decays on 10 and 220 fs time scales and recovers on a time scale much longer than the experimental time delay. X and GS* form in <20 fs and decay on a ~230 fs time scale. The intermediate $[Fe^{III}(CN)_5]^{2-}$ species grows on a slower time scale (~240 fs) and decays on a similar time scale (~76 ps) as the formation of $[Fe^{III}(CN)_5(CH_3OH)]^{2-}$ (the decay is not shown in Figure 6c). Because IR signatures and accurate absorbance cross sections for the three intermediates are not available, Figure 6c is in relative concentration units taken directly from the results of the model (i.e., $c_{GS}(t = 0) = 1$).

The role of the metastable linkage isomers in NO photodissociation is often discussed in the literature. Our data analysis shows that the photorelease of NO· competes with photoinduced metastable linkage isomerism in SNP. As shown in Scheme 1, these two pathways share common excited state(s) labeled as GS* and X. After absorbing one-photon and reaching state(s) GS*, the NO ligand in SNP can undergo a 180° rotation to form the MS1 isomer or photodissociate to form NO radical. Alternatively, SNP can absorb another photon to reach an intermediate state X. These intermediate states are viewed to be highly delocalized multidimensional potential energy surfaces with many surface crossings. From this X state, the primary pathway is NO release with a small portion of the population relaxing into MS2 by rotation of the NO ligand by 90°. This agrees with our experimental data and takes into account that MS1 is formed via a one-photon process, MS2 is formed via a two-photon process, and NO· is generated from a combination of one- and two-photon pathways.

Comparison with Previous Studies. As noted earlier, most studies of photoinduced linkage isomerism in SNP and other related metal−nitrosyl compounds have been done at low temperature in the solid state. We expect that the hydrogen-bonding interactions of methanol and SNP will significantly impact the photochemistry of SNP at room temperature by stabilizing/destabilizing highly excited intermediate states and/or the metastable product states. Keeping this in mind, we compare the major findings of our experiment with previous photochemical studies of SNP.

The role of MS1 and MS2 in the photorelease of NO· in metal−nitrosyl photochemistry has been studied by various groups, and there are two main mechanisms that have been suggested in the literature, one of which involves competing processes leading to either linkage isomerism or photorelease of NO· and the other involves nitrosyl ligand dissociation following linkage isomerism in a two-step consecutive mechanism. In a recent review on photoactive ruthenium nitrosyls, the authors suggest that NO· may be generated through a consecutive mechanism where the nitrosyl ligand is dissociated from either MS1 or MS2.[6] In this scenario, MS1 and MS2 are transient species that are depleted to generate NO·. This consecutive mechanism has been considered by Dieckmann et al. who observed phototriggered (λ_{pump} = 532 nm) nitric oxide and cyanide release from SNP molecules deposited on thin films at 294 K.[71] Although they were not able to detect either MS1 or MS2, they modeled their data using a two-step NO· release process, suggesting the linkage isomers as intermediate species. Einarsdóttir and co-workers measured a transient state from which they observed NO· photorelease in flash photolysis experiments (λ_{pump} = 355 nm) on a Ru nitrosyl compound in aqueous solution at 298 K.[72] They attributed the transient intermediate state formed within ≤100 ns to either MS1 or MS2. Giglmeier et al. observed the production of MS1, MS2, and NO photorelease using FTIR spectroscopy after photoexciting single crystals of a Ru nitrosyl porphyrin.[9] The authors were not able to conclusively determine whether photoisomerization and photodissociation were occurring in a consecutive manner (i.e., formation of NO from a metastable state), if the processes were competing, or if there was no relation between the photochemical processes at all. On the basis of the studies mentioned above and others, the role of MS1 and MS2 in the overall photochemistry of SNP remains unclear, although it is possible that different experimental conditions lead to different photochemical outcomes.

Our experiment is able to measure the formation and dynamics of MS1, MS2, and NO· in solution at room temperature, and our results demonstrate that photoinduced linkage isomerism and photodissociation are in fact competing processes, as

dx.doi.org/10.1021/ja110881n |J. Am. Chem. Soc. 2011, 133, 5255–5262

shown in Scheme 1 and Figure 6. Note that our data do not support the idea that MS1 and MS2 are intermediate species in NO photodissociation. If this were the case, we would observe a depletion of the population of MS1 and MS2 over the course of our experiment, which we do not. In our model, GS* and X represent complex potential energy surfaces from where the molecule can undergo linkage isomerism (minor pathway) or photodissociation (major pathway).

It is important to point out that the UV pump power dependence we observed in this experiment is different from what is currently in the literature.[1,54,55] Most previous experiments have employed excitation light in the range of 450−530 nm followed by longer wavelength irradiation to efficiently trap one or more linkage isomers at low temperatures. In the present experiment utilizing 400 nm pump pulses, we have observed that we can form MS1 with one photon, and that it takes two photons to form MS2 at room temperature in solution. Our results demonstrate that given the right excitation conditions and high detection sensitivity, it is possible to observe both MS1 and MS2 linkage isomers at room temperature.

Previous steady-state photochemical studies of SNP in solution at room temperature have measured the primary photoproduct to be $[Fe^{III}(CN)_5(solvent)]^{2-}$ (solvent = CH_3OH, H_2O).[45,47,48] Other dissociation products such as NO, CN, and Prussian blue are also observed by infrared spectroscopy and mass spectrometry. Because of the steady-state nature of these experiments, the metastable states MS1 and MS2 were not observed. In this study, we are able to observe all the photochemical products listed above in a time-resolved manner. This allows us to measure the solvent association time scale of $[Fe^{III}(CN)_5(CH_3OH)]^{2-}$ to be 130 ps and the formation time of Prussian blue to be 320 ps. Our model suggests that MS1, MS2, and NO· are formed within ∼300 fs and decay on a ∼100 ns time scale.

CONCLUDING REMARKS

The high structural sensitivity of transient infrared spectroscopy has allowed the simultaneous detection of the photoinduced MS1 ($[Fe^{II}(CN)_5(\eta^1\text{-ON})]^{2-}$) and MS2 ($[Fe^{II}(CN)_5(\eta^2\text{-NO})]^{2-}$) linkage isomers of SNP and the photodissociated free nitrosyl radical at room temperature in a methanol solution. These three transient species are detected using their distinct nitrosyl stretching frequencies at 1794 cm^{-1} (MS1), 1652 cm^{-1} (MS2), and 1851 cm^{-1} (NO·). Additional photodissociation products including the cyanide ion, $[Fe^{III}(CN)_5(CH_3OH)]^{2-}$, and Prussian blue are measured. The UV-pump power dependence enabled the development of a kinetic model involving a one-photon absorption pathway to MS1, a two-photon absorption pathway to MS2, and a combination of both one- and two-photon absorption processes leading to the photodissociation products including free NO radical. Our results suggest that photoisomerization of MS1 and MS2 and photodissociation of NO are competing pathways in the photochemistry of SNP at room temperature.

The results from our experiments demonstrate that the photochemistry of metal−nitrosyl complexes in solution at room temperature (most relevant to chemistry and biology) needs further attention from theorists and experimentalists alike. The above findings have implications for the photochemistry of transition metal−nitrosyl compounds, the design of optical devices based on the metastable isomers, the photodelivery of NO in medicine, and the understanding of M−NO bonding in metalloproteins.

ASSOCIATED CONTENT

Supporting Information. Bleach dynamics, kinetic fitting parameters, full details of the kinetic model presented in Scheme 1, integrated molar absorptivity calculations, and complete ref 65. This material is available free of charge via the Internet at http://pubs.acs.org.

AUTHOR INFORMATION

Corresponding Author
mkhalil@chem.washington.edu

ACKNOWLEDGMENT

This work was supported by the Office of Basic Energy Sciences of the U.S. Department of Energy (Grant No. DE-SC0002190) and the National Science Foundation under CHE-0847790. M. K. acknowledges support from the Camille and Henry Dreyfus New Faculty Award and the David and Lucille Packard Fellowship for Science and Engineering.

REFERENCES

(1) Coppens, P.; Novozhilova, I.; Kovalevsky, A. *Chem. Rev.* **2002**, *102*, 861–883.
(2) Fomitchev, D.; Novozhilova, I.; Coppens, P. *Tetrahedron* **2000**, *56*, 6813–6820.
(3) Coppens, P.; Fomitchev, D.; Carducci, M. D.; Culp, K. *J. Chem. Soc., Dalton Trans.* **1998**, 865–872.
(4) Bitterwolf, T. E. *Coord. Chem. Rev.* **2006**, *250*, 1196–1207.
(5) Gutlich, P.; Garcia, Y.; Woike, T. *Coord. Chem. Rev.* **2001**, *219−221*, 839–879.
(6) Rose, M.; Mascharak, P. *Coord. Chem. Rev.* **2008**, *252*, 2093–2114.
(7) Hayton, T. W.; Legzdins, P.; Sharp, W. B. *Chem. Rev.* **2002**, *102*, 935–992.
(8) Bitterwolf, T. E. *Inorg. Chem. Commun.* **2008**, *11*, 772–773.
(9) Giglmeier, H.; Kerscher, T.; Klüfers, P.; Schaniel, D.; Woike, T. *Dalton Trans.* **2009**, 9113–9116.
(10) Xu, N.; Yi, J.; Richter-Addo, G. B. *Inorg. Chem.* **2010**, *49*, 6253–6266.
(11) Cheng, L.; Novozhilova, I.; Kim, C.; Kovalevsky, A.; Bagley, K.; Coppens, P.; Richter-Addo, G. *J. Am. Chem. Soc.* **2000**, *122*, 7142–7143.
(12) Fomitchev, D. V.; Coppens, P.; Li, T. S.; Bagley, K. A.; Chen, L.; Richter-Addo, G. B. *Chem. Commun.* **1999**, 2013–2014.
(13) Novozhilova, I. V.; Coppens, P.; Lee, J.; Richter-Addo, G. B.; Bagley, K. A. *J. Am. Chem. Soc.* **2006**, *128*, 2093–2104.
(14) Nutt, D. R.; Karplus, M.; Meuwly, M. *J. Phys. Chem. B* **2005**, *109*, 21118–21125.
(15) Nutt, D. R.; Meuwly, M. *ChemPhysChem* **2007**, *8*, 527–536.
(16) Hauser, U.; Oestreich, V.; Rohrweck, H. D. *Z. Phys. A* **1977**, *280*, 17–25.
(17) Zöllner, H.; Krasser, W.; Woike, T.; Haussühl, S. *Chem. Phys. Lett.* **1989**, *161*, 497–501.
(18) Pressprich, M. R.; White, M. A.; Coppens, P. *J. Am. Chem. Soc.* **1993**, *115*, 6444–6445.
(19) Pressprich, M. R.; White, M. A.; Vekhter, Y.; Coppens, P. *J. Am. Chem. Soc.* **1994**, *116*, 5233–5238.
(20) Carducci, M. D.; Pressprich, M. R.; Coppens, P. *J. Am. Chem. Soc.* **1997**, *119*, 2669–2678.
(21) Morioka, Y.; Saitoh, H.; Machida, H. *J. Phys. Chem. A* **2002**, *106*, 3517–3523.

(22) Schaniel, D.; Imlau, M.; Weisemoeller, T.; Woike, T.; Kraemer, K. W.; Guedel, H. *Adv. Mater.* **2007**, *19*, 723–726.
(23) Imlau, M.; Woike, T.; Schaniel, D.; Schefer, J.; Fally, M.; Rupp, R. A. *Opt. Lett.* **2002**, *27*, 2185–2187.
(24) Imlau, M.; Woike, T.; Schieder, R.; Rupp, R. A. *Phys. Rev. Lett.* **1999**, *82*, 2860–2863.
(25) Imlau, M.; Haussuhl, S.; Woike, T.; Schieder, R.; Angelov, V.; Rupp, R. A.; Schwarz, K. *Appl. Phys. B: Lasers Opt.* **1999**, *68*, 877–885.
(26) Woike, T.; Haussuehl, S.; Sugg, B.; Rupp, R. A.; Beckers, J.; Imlau, M.; Schieder, R. *Appl. Phys. B: Lasers Opt.* **1996**, *63*, 243–248.
(27) Schuy, A.; Woike, T.; Schaniel, D. *J. Sol-Gel Sci. Technol.* **2009**, *50*, 403–408.
(28) Butler, A. R.; Glidewell, C. *Chem. Soc. Rev.* **1987**, *16*, 361–380.
(29) Hollenberg, S. M. *Heart Failure Rev.* **2007**, *12*, 143–147.
(30) Shin David, D.; Brandimarte, F.; De Luca, L.; Sabbah Hani, N.; Fonarow Gregg, C.; Filippatos, G.; Komajda, M.; Gheorghiade, M. *Am. J. Cardiol.* **2007**, *99*, 4A–23A.
(31) Ford, P. C.; Wecksler, S. *Coord. Chem. Rev.* **2005**, *249*, 1382–1395.
(32) Schaniel, D.; Woike, T. *Phys. Chem. Chem. Phys.* **2009**, *11*, 4391–4395.
(33) Woike, T.; Krasser, W.; Bechthold, P. S.; Haussuehl, S. *Solid State Commun.* **1983**, *45*, 503–506.
(34) Woike, T.; Krasser, W.; Bechthold, P. S.; Haussuehl, S. *Solid State Commun.* **1983**, *45*, 499–502.
(35) Krasser, W.; Woike, T.; Bechthold, P. S.; Haussuehl, S. *J. Mol. Struct.* **1984**, *114*, 57–60.
(36) Zoellner, H.; Woike, T.; Krasser, W.; Haussuehl, S. *Z. Kristallogr.* **1989**, *188*, 139–153.
(37) Schaniel, D.; Woike, T.; Schefer, J.; Petricek, V.; Kramer, K. W.; Gudel, H. U. *Phys. Rev. B* **2006**, *73*, 174108.
(38) Schaniel, D.; Woike, T.; Schefer, J.; Petricek, V. *Phys. Rev. B* **2005**, *71*, 174112.
(39) Güida, J. A.; Aymonino, P. J.; Piro, O. E.; Castellano, E. E. *Spectrochim. Acta, Part A* **1993**, *49*, 535–542.
(40) Villalba, M. E. C.; Guida, J. A.; Varetti, E. L.; Aymonino, P. J. *Spectrochim. Acta, Part A* **2001**, *57A*, 367–373.
(41) Villalba, M. E. C.; Gueida, J. A.; Varetti, E. L.; Aymonino, P. J. *Inorg. Chem.* **2003**, *42*, 2622–2627.
(42) Schefer, J.; Woike, T.; Imlau, M.; Delley, B. *Eur. Phys. J. B* **1998**, *3*, 349–352.
(43) Schaniel, D.; Schefer, J.; Delley, B.; Imlau, M.; Woike, T. *Phys. Rev. B* **2002**, *66*, 085103.
(44) Schaniel, D.; Woike, T.; Merschjann, C.; Imlau, M. *Phys. Rev. B* **2005**, *72*, 195119.
(45) Wolfe, S.; Swinehart, J. *Inorg. Chem.* **1975**, *14*, 1049–1053.
(46) Kudo, S.; Bourassa, J. L.; Boggs, S. E.; Sato, Y.; Ford, P. C. *Anal. Biochem.* **1997**, *247*, 193–202.
(47) Deoliveira, M.; Langley, G.; Rest, A. *J. Chem. Soc., Dalton Trans.* **1995**, 2013–2019.
(48) Stochel, G.; Stasicka, Z. *Polyhedron* **1985**, *4*, 481–484.
(49) Manoharan, P. T.; Gray, H. B. *J. Am. Chem. Soc.* **1965**, *87*, 3340–3348.
(50) Ishikawa, T.; Tanaka, K. *J. Chem. Phys.* **2005**, *122*, 074314.
(51) Ishikawa, T.; Tanaka, K. *Z. Kristallogr.* **2008**, *223*, 334–342.
(52) Boulet, P.; Buchs, M.; Chermette, H.; Daul, C.; Furet, E.; Gilardoni, F.; Rogemond, F.; Schlaepfer, C. W.; Weber, J. *J. Phys. Chem. A* **2001**, *105*, 8999–9003.
(53) Boulet, P.; Buchs, M.; Chermette, H.; Daul, C.; Gilardoni, F.; Rogemond, F.; Schlaepfer, C. W.; Weber, J. *J. Phys. Chem. A* **2001**, *105*, 8991–8998.
(54) Buchs, M.; Daul, C.; Manoharan, P. T.; Schläpfer, C. *Int. J. Quantum Chem.* **2003**, *91*, 418–431.
(55) Delley, B.; Schefer, J.; Woike, T. *J. Chem. Phys.* **1997**, *107*, 10067–10074.
(56) Sando, G. M.; Zhong, Q.; Owrutsky, J. C. *J. Chem. Phys.* **2004**, *121*, 2158–2168.
(57) Stamler, J. S.; Singel, D. J.; Loscalzo, J. *Science* **1992**, *258*, 1898–1902.
(58) Experimentally determined from the 2D IR spectrum of SNP in methanol.
(59) This value cannot be determined accurately due to the maximum time delay of 0.5 ns.
(60) Upon prolonged excitation at 400 nm, a bleach appears at 2100 cm^{-1} corresponding to formation of Prussian blue.
(61) Independently determined from the FTIR spectrum of KCN in methanol.
(62) Shanoski, J. E.; Glascoe, E. A.; Harris, C. B. *J. Phys. Chem. B* **2006**, *110*, 996–1005.
(63) Fisher, J.; Susumu, K.; Therien, M.; Yodh, A. *J. Chem. Phys.* **2009**, *130*, 134506.
(64) Calculated at the BP86 level of theory with 6-31G(d) for iron atoms and 6-311+G(3df) for all other atoms. All calculations were performed using the polarizability continuum model with a methanol dielectric.
(65) Frisch, M. J.; et al. *Gaussian 03*, revision C.02; Gaussian, Inc.: Wallingford, CT, 2004.
(66) Smith, A. L.; Keller, W. E.; Johnston, H. L. *J. Chem. Phys.* **1951**, *19*, 189–192.
(67) Kim, S.; Heo, J.; Lim, M. *Bull. Korean Chem. Soc.* **2005**, *26*, 151–156.
(68) Nakamoto, K. *Infrared and Raman Spectra of Inorganic and Coordination Compounds*, 4th ed.; John Wiley and Sons: New York, 1986.
(69) Estrin, D. A.; Baraldo, L. M.; Slep, L. D.; Barja, B. C.; Olabe, J. A.; Paglieri, L.; Corongiu, G. *Inorg. Chem.* **1996**, *35*, 3897–3903.
(70) Schaniel, D.; Nicoul, M.; Woike, T. *Phys. Chem. Chem. Phys.* **2010**, *12*, 9029–9033.
(71) Dieckmann, V.; Imlau, M.; Taffa, D. H.; Walder, L.; Lepski, R.; Schaniel, D.; Woike, T. *Phys. Chem. Chem. Phys.* **2010**, *12*, 3283–3288.
(72) Szundi, I.; Rose, M.; Sen, I.; Eroy-Reveles, A. A.; Mascharak, P.; Einarsdóttir, O. *Photochem. Photobiol.* **2006**, *82*, 1377–1384.